Proceedings of the 5th International Conference on Fluid Flow and Thermal Science (ICFFTS 2024)
Lisbon, Portugal- November 21 - 23, 2024
Paper No. 114
DOI: 10.11159/icffts24.114

Graphical and Statistical Analysis of Nonlinear Internal Wave Dynamics Using Spatio-Temporal Array Observations: Preliminary Results

Nicholas V. Scott[1], Jeffrey W. Book[2], and Katherine Seery[1]
[1]Apogee Engineering, LLC, Science and Technology Group
2661 Commons Blvd., Suite 200, Beavercreek, Ohio 45431, USA
nicholas.scott@apogeeusa.com; bookatsea@gmail.com; katherine.seery@apogeeusa.com
[2]Naval Research Laboratory, Oceanography Division
Stennis Space Center, MS 39529, USA

Abstract – Tidally driven internal wave packets are an important dynamical process influencing mixing of nutrients, salinity, and temperature in coastal waters over daily, weekly, monthly, and seasonal time scales. Past parameterization of nonlinear internal wave dynamics off the northwest coast of Australia included time dependent empirical orthogonal function analysis which successfully quantified temperature fluctuations in the water column over a semidiurnal time scale. Seasonal time scale internal wave analysis has been carried out using an array of pressure measurements distributed over the same continental shelf area and using a variety of statistical algorithms. Over a 4-month time span Bayesian belief networks, quantifying covariance between mooring-based observation posts, demonstrate an indirect wave signal propagation pathway between posts suggesting the influence of the bottom boundary layer on spatial internal wave coherence. The use of Wiener filtering, least mean square filtering, and hidden Markov modeling between observation posts separated in space suggests anisotropic wave signal propagation consistent with the M2 barotropic propagation of energy from west to east along the continental shelf. High energy pressure event statistical estimation using Morlet wavelet analysis, a parameterization of steep internal wave groups, shows strong local maxima at distinct local time scales of 1-2 days and 15 days at different nodes. Further analysis of maximum wave pressure events reveals a strong fit to the generalized extreme value distribution consistent with the shape parameter varying with each observation post. Bayesian belief networks for maximum pressure energy values show a nodal-edge structure different from the Bayesian belief network previously calculated parameterizing both low and high energy pressure waves. Strong edge connections exist primarily for adjacent observation posts suggesting possible steep wave attenuation. In addition, the Bayesian belief network has arrows pointing in the direction opposite to the general M2 barotropic energy flux. All extreme value statistical results are consistent with the impact of hurricanes Iggy and Lua causing disruption of the general flow of wave energy.

Keywords**:** internal waves, Bayesian belief network, hidden Markov model, Morlet wavelet transform, extreme values, observation post, covariance

1. Introduction

Coastal internal waves are a pervasive motion on the northwest coast of Australia responsible for augmented mixing levels of fluid tracers and momentum as well as being a crucial component in wave-wave interactions and other modulations in oceanic motions on a variety of time scales. Previous research has focused on the quantification of the flow variability over short time scales using a sequence of moorings placed along the continental shelf [1]. One thing suggested from this study is the importance of understanding the dynamical structure of nonlinear internal wave packets over longer time scales which can impact processes important to human life such as continental shelf change, gas/heat flux modulation, and climate change. As an alternative to traditional methods of looking at arrays of point measurements, a statistical machine learning analytical approach is used to investigate and gain preliminary insight into a series of physical oceanographic questions. First, what covariance-based relationship do internal wave packets at one point in space have with one another? Second, how does this relationship compare with known understanding of wave energy fluxes in the domain? Finally, what is the structure of extreme waves and how is their covariance-based relationship similar or different to an internal wavefield comprised of all waves (both large and small amplitude waves). This paper attempts to address these questions using a variety of signal processing and statistical machine learning techniques including Bayesian belief networks (BBNs), linear adaptive filtering, hidden Markov modeling, and Morlet wavelet analysis-based high energy event quantification. After a brief description of the data and analytical methods is provided, results are given which provide preliminary insight into the spatial nonlinear

internal wave structure. It is through this analysis that evidence for the feasibility of this nontraditional approach is demonstrated, paving the way for alternate ways of looking at nonlinear internal waves.

2. Field Data Structure and Data Analysis Methods

2.1. Pressure Data Acquired From Nodal Array

The pressure data analyzed was acquired from mooring nodes 1, 2, and 3 situated in space as shown in Figure 1. Each mooring node constituted a series of instruments capturing many oceanographic variables include temperature, velocity, pressure, and salinity. The data analyzed in this work comprised pressure measurements from underwater pressure sensors acquired at 6 unique spatial points or observation posts. Each mooring node possessed 2 observation posts at two different depths. At each observation post 257 mean pressure samples where measured at a frequency of twice day with a sampling interval of 12 hours. The mean and maximum values over these pressure sample realizations were taken at each measurement time at each observation post to form two different internal wavefield feature matrices each consisting of 257 rows and 6 columns. The rows of each matrix designate mean or maximum pressure values over time, and the columns delineate pressure measurements taken at the 6 distinct observation posts. Pressure measurements were acquired from approximately 12/28/2011 to 4/1/2012. Figure 2 shows 6 rectangles where each vertical column of rectangles represents the mooring nodes 1 to 3 from left to right in Figure 1. The depths of the pressure measurements appear as labels next to the rectangles. Though pressure data measurements were taken twice a day at each observation post, the measurements at all 6 sampling points were not taken strictly cotemporally. During the data acquisition period the northwest coast of Australia experienced two hurricanes - hurricanes Iggy and Lua. Hurricanes Iggy and Lua impacted the measurement area during the time period of 3/11/2011 -3/12/2011 and 4/2/2011- 4/3/2011 respectively.

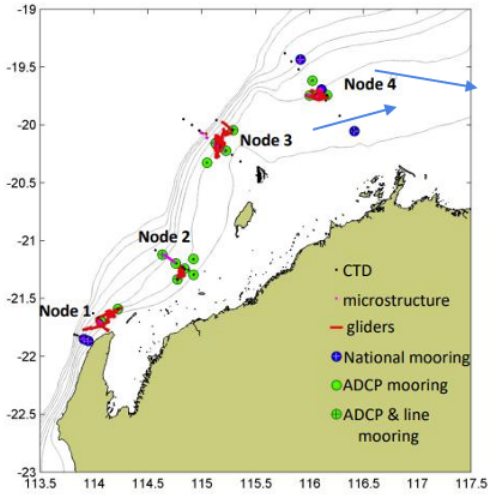

Figure 1: Map of 4 mooring nodes deployed in 2011/2012 field experiment. Data from nodes 1-3 were used in this work. The 50 m, 100 m, 150 m, 200 m, 300 m, 400 m, and 500 m isobath contours are drawn in gray. Horizontal and vertical scales are longitude and latitude respectively. Figure taking from Book et. al (2016).

2.2. Major Data Processing Methodologies

BBNs are probabilistic graphical models which use network edges and nodes to model the joint probability distribution existing between a set of random variables describing a system [2]. (The term network node is used here in the graphical network sense and is distinct from the term mooring node as used above in reference to observation posts for

oceanographic moorings). Prior to statistical inference, network nodes along with nodal states require definition followed by structural learning which derives the directed acyclic graph (DAG) associated with the BBN. The structural learning process exhumes BBN topology from the data. With the discovery of network structure, parameter learning can be performed which provides numerical values to conditional probabilities existing between network nodes [3]. The defined network nodes and conditional probabilities provide for statistical inference where the effects of evidence at one or more random variable network nodes are propagated throughout the BBN to estimate its impact on others.

BBN analysis was performed on pressure matrix data using the software package Bayes Server manufactured by Bayes Server Ltd. which automates much of the statistical analysis including the BBN structural and parameter learning. The Chow-Liu structural learning algorithm was used in this work which is a global structural learning method which searches network structures using a single root initial network structure in the beginning of the network learning process [4]. Variations from this network structure are performed at each step causing the tree to increase in complexity. The tree structure model used is a multivariate probability distribution expressed as a product of conditional probability distributions based on a parent node in the tree. The tree structure that best approximates the real distribution is found by minimizing the difference between the real data-based distribution and the tree approximation. This is done by minimizing the mutual information between any two pairs of network nodal variables [2]. The best network structure, in other words, is selected based on a score measuring how well the model represents the data. The Chow-Liu algorithm assumes a tree structural model appropriate to the data via seeking an edge-node structure consisting of a low number of dominant parental nodes which provide sub-dominant children nodes. The direction of links is found using higher order dependency tests [5]. Parameter learning provides numerical values to the nodal-edge structure allowing for statistical inference between nodes. This is done using a relevance tree algorithm which allows for exact statistical inference rather than approximate inference [5].

A hidden Markov model (HMM) is a double stochastic process consisting of a Markov chain hidden state stochastic process, which is not directly observable, and an observation stochastic process which is observable. In addition to the memoryless Markov property of the state stochastic process, the HMM possesses the stationarity property, where the transition and observation probabilities do not change over time, and observation independence, where the observations only depend on current state [6]. The HMM is a probabilistic graphical model where states and observations are random variables such that each state transitions to another state and emits only one observation for each state. The statistical relationship between states is parameterized via a state transition matrix A, while the relationship of states to observations is parameterized via an emission matrix B [7]. The HMM is applied to pressure measurements, X and Y, from two observation posts where X is considered the state variable and Y the observation variable. The parameters of the HMM are estimated by taking the values in each of these pressure measurement variables and dividing them up into intervals where the transition frequency between state intervals in X is counted along with the calculation of the probability distribution for observation variable intervals for Y when the state transition is made. This is called instance counting and is simply a method for counting the number of state transitions and observation emissions associated with each state transition [8]. A fully parameterized HMM, consisting of transition and emission matrices, allows for the statistical prediction of observations or pressure values at one observation post given pressure value change at another.

The continuous Morlet wavelet transform, designated by WP(a, t) is implemented in a discretized form for pressure value analysis and enables the tracking of coherent structures in a pressure signal at each observation post [9]. The Morlet wavelet transform was performed over a set of discrete scales with logarithmic spacing extending from 24 hours to 1260 hours. This period range was found via inspection of the Morlet wavelet transform of the pressure time series at the observation posts to find the range that carried the largest number of high energy pressure events. The Morlet wavelet transform of a pressure signal, WP(a, t) produces a measure of the average pressure energy over the support of the wavelet. In other words, a pressure signal containing a large amplitude or energy pressure event at scale a_0 and time t_0 will have a wavelet transform characterized by a large peak value of WP at (a_0, t_0), and the peak value is proportional to the average pressure energy of the signal over the support of the wavelet in the neighborhood of t_0. The traditional energy scaling of the Morlet wavelet transform facilitates the detection of high-pressure events in internal wavefield pressure signals.

The extracted pressure time-series are subject to edge effects at the boundaries, especially at large scales, due to the 'start up' effect of the convolution which is part of the Morlet wavelet transform. This edge effect takes the form of a cone of influence which produces a linearly decreasing region of contamination as the scale is decreased [10]. To account partially for statistical bias introduced by edge effect contamination, five days' worth of data at the beginning and end part of the Morlet transform were not included in the statistical calculation to follow. This truncated region takes into account the scale region where most (but not all) of the high energy pressure events occur. Due to the limited length of the time series, more data could not be discarded.

The wavelet transform contains an array of high energy pressure events designated by local maxima. To obtain a distribution of these events, the 95% significance level of points in the WP(a,t) time-scale space were calculated. This region provides a subset of points in time-scale space where a constant wavelet energy threshold was applied using a pressure energy threshold range. This threshold range varied depending on the observation post pressure time series analyzed and was found by inspection of WP(a,t) time-scale space. From these groups of points, the highest energy pressure values were found. The highest pressure values or local maxima throughout the wavelet transform domain were obtained using a nine-point box filter. The filter was moved throughout the time-scale space and only those points that are larger than the surrounding eight points in 95% significance level subset of points were selected. This is the same technique used by Scott [11] and Scott et al. [12]. The high energy pressure events have associated scale values and time positions which admit a statistical distribution dubbed the high-pressure event statistic $P_H(T)$ which is a function of time period T and pressure threshold H.

3. Results

Previous oceanographic analysis using BBNs applied to point measurements in a turbulent flow field have been performed. Scott and Kulkulka [13] performed BBN analysis on large eddy simulation turbulent shear flow data and demonstrated convoluted pathways of covariance and joint probability distributions associated with horizontally distributed localized fluctuations of temperature and turbulent kinetic energy. The application of the Chow-Liu algorithm to horizontally and vertically distributed pressure field measurements demonstrate evidence of a west to east trend for the M2 tidal barotropic energy flux direction. However, the BBN also reveals complex pathways for pressure covariance as shown in Figure 2. Edge-nodal connections show a pathway that descends from observation post 1 to 4 which is directly under it where the mutual information value between the nodes is 0.1. (Mutual information is a metric for quantifying the strength of an edge connection which varies from 0 to 1 where 1 delineates high covariance or mutual information). Observation post 4 is then connected to the adjacent observation post 5 with a mutual information value of 0.9 followed by a vertical connection upward to observation post 2. The mutual information value connection observation post 5 and 2 is 0.7.

Though the downward flux of wave signal information is relatively weak, the full pathway demonstrates how pressure information follows a non-direct, circuitous pathway from observation post 1 to 2. A possible reason for the presence of this pathway is the influence of the bottom boundary layer along the continental shelf. Internal tides are associated with the movement of the entire water column cyclically over a day where ocean waters are dragged along the ocean bottom. The semidiurnal tidal forcing can produce internal wave packet fluctuations allowing for the dominant wave signal pathway connecting observation post 1 and 2 to be along the sub-surface pathway connecting observation posts 4 and 5. In this situation tidal forcing-based energy sweeps from left to right in Figure 2 where significant signal covariance is fostered between observation posts 4 and 5 by bottom generated eddies. These bottom generated eddies tend to propagate upward towards the surface accounting for the covariance between observation posts 5 and 2. The influence of the bottom boundary layer is also suggested by the edge connecting observation post 6 and 3 where the BBN structure again suggests that probabilistic pressure information flows upward towards the surface from sub-surface waters. A long spatial connection of observation post 1 to 6 does exists where a significant part of the BBN is in the west to east direction. This structure may suggest a long range M2 tidal flux.

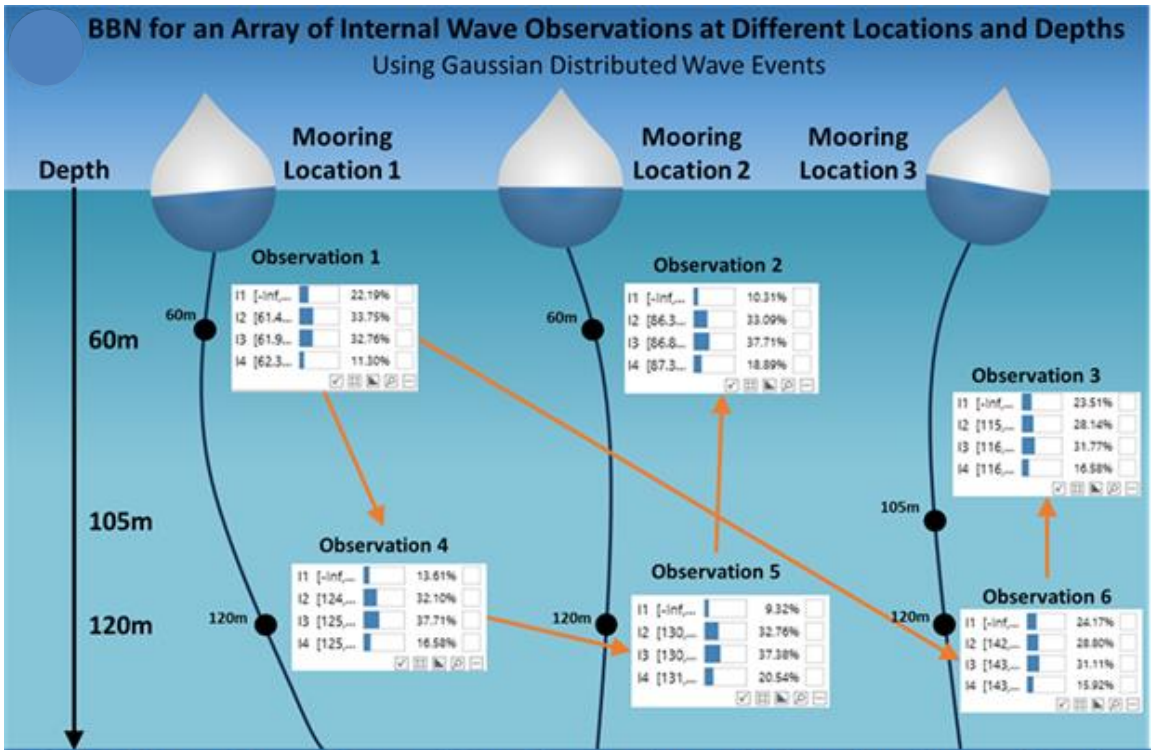

Figure 2: BBN for pressure measurements captured by a mooring array situated off the northwest coast of Australia. Mooring nodes 1, 2, and 3 designated by vertical mooring columns of rectangular observations posts delineated by the rectangles. Pressure levels in arbitrary units are shown inside the rectangles. West and east are on the left and right sides respectively. Depth labels for each observation post appear next to each rectangle. Edge connections displayed as arrows. The distributions of pressure for the observation posts are Gaussian. No BBN evidential instantiations have been applied.

Independent statistical analyses can substantiate the direction of the edge connections of the BBN. Wiener filtering and least mean square (lms) filtering were performed between observation posts 1 and 6 where observation post 1 and 6 were taken as the system input and output respectively [14]. Wiener filtering and least mean square filtering was also performed between observation posts 3 and 4 where observation post 3 and 4 were taken as the system input and output respectively. Note that no edge connection exists between these observation posts. The objective of this analysis is to examine the west-to-east and east-to-west information propagation system structure to see if alternative algorithms can suggest which energy direction is physically appropriate. Figure 3 a)-b) shows the results of the statistical signal processing where 10 tap Wiener and lms filters were estimated. The system filters connecting observation posts 1 and 6 are smooth with a gradual decrease in filter potency with increasing filter taps. This filter models the direction of the semidiurnal internal tide energy flux which is west to east. On the other hand, the system filter connecting observation posts 3 and 4 are noisy and erratic for the Wiener filter and almost flat for the lms filter. The filters in this case models energy flux in the opposite direction of east to west. The structure of the filters is consistent with the known direction of wave signal information movement being west-to-east which is also consistent with the graphical structure of the BBN.

Hidden Markov model parameter estimation of transition and emission matrices for the same observation posts used in the adaptive filtering modeling was performed. Figures 4 a)-b) displays the transition and emission matrices for observation posts 1 and 6 where observation post 1 is the state variable and observation post 6 is the observation variable. Figures 4 c)-d) displays the transition and emission matrices for observation posts 3 and 4 where observation post 3 is the

state variable and observation post 4 is the observation variable. The transition matrices for both systems display the typical structure where state transitions from one level are probabilistically related to adjacent state levels which are forward and backward or to right and left for each horizontal state interval. For instance, Figure 4 a) shows an array of discrete state levels over the range -1.0 to 1.5 for observation post 1. The discrete pressure state level of 0-0.5 has the highest probability of transitioning into itself with significantly lower probability of transitioning into -0.5 to 0 and 0.5 to 1.0. The emission matrix parameterizing the dynamics of observation post 1 as a state variable and observation post 6 as the observation variable shows a peaked probability structure where high probability values are along the diagonal. However, the same tight probability distribution is not displayed for the system consisting of the state variable of observation post 3 and the observation variable of observation post 4. Figure 4c) displays a tridiagonal structure for the state variable taken as observation 3. This form is similar structure observed in Figure a). However, the peaked probability distribution structure is not seen for the state-observation variable emission matrix consisting of observation post 3 and 4 in Figure 4d). The emission matrix is very noisy and the probability density function for each state level (the emission matrix rows) contains variance spread out over many intervals. The wideness of the distribution for each row suggests that the system model does not capture the true wave flux of energy/information.

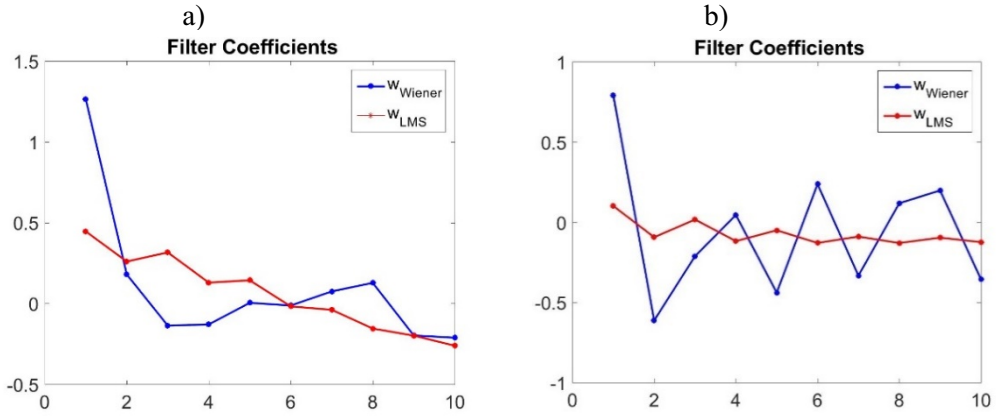

Figure 3: Adaptive filter-based system identification relating pressure measurements at two different observation posts. Ten tap filter coefficients shown for Wiener and lms filters. a) System filter coefficients for observation posts 1 and 6 where posts 1 and 6 are the input and output variables respectively. b) System filter coefficients for observation posts 3 and 4 where posts 3 and 4 are the input and output variables respectively.

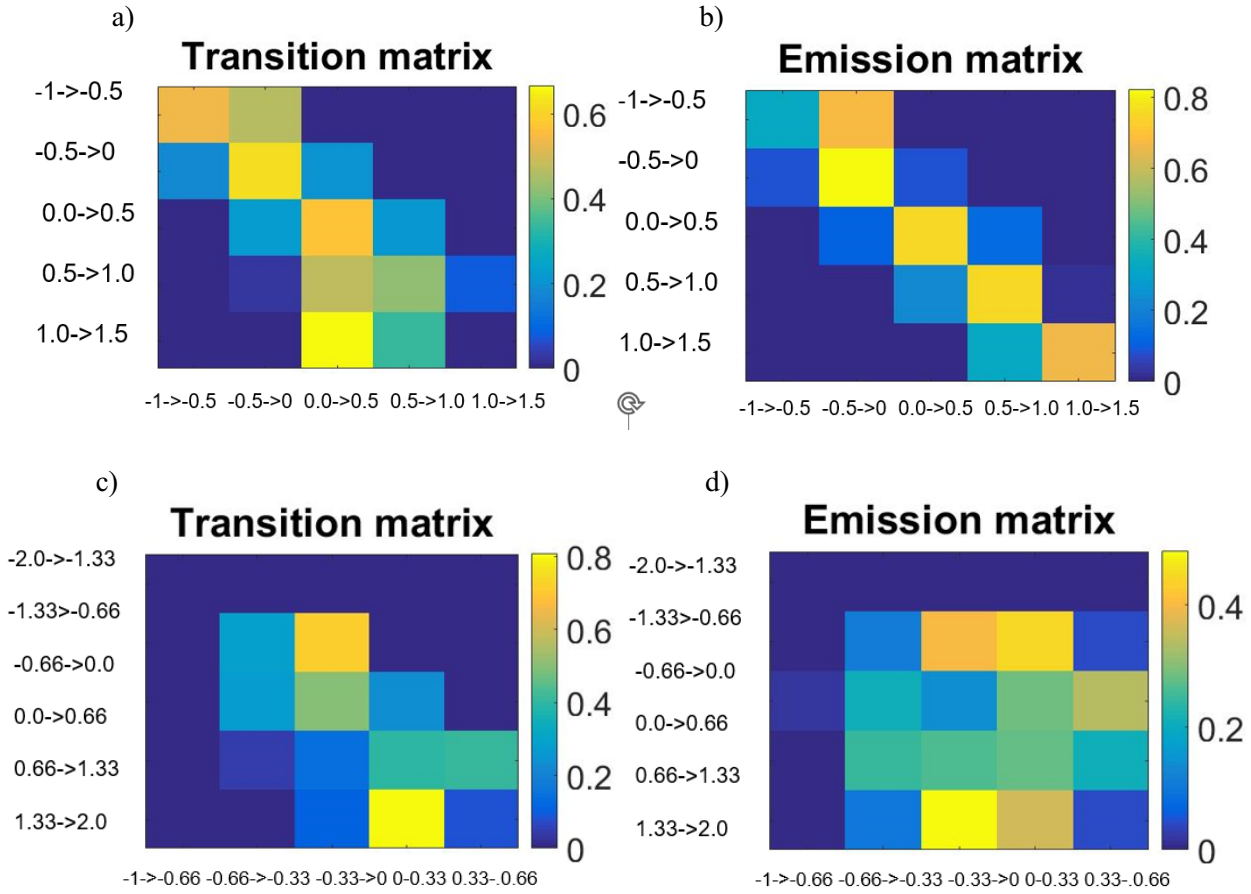

Figure 4: Transition and emission matrices for two different bi-nodal variables. a) Transition matrix for observation post 1. b) Emission matrix for state variable of observation post 1 and observation variable of observation post 6. c) Transition matrix for observation post 3. d) Emission matrix for state variable of observation post 3 and observation variable of observation post 4. State and observation variable pressure intervals on the vertical and horizontal axes respectively. Each row for the emission matrices sums to 1 making it a true probability distribution.

Extreme pressure events exist in the measured pressure wave field caused in part by the two hurricanes moving in the vicinity of the measurement area. The maximum value wave pressure distributions at each of the observation posts all possess generalized extreme value distributions with shape parameters that varied over a range of [-0.28 0.05] [15]. This substantiates that the maximum pressure values reflect variable extreme value statistical dynamics over the complete measurement region. The fraction of high energy pressure events as a function of period scale based on the use of Morlet wavelet analysis is shown in Figures 5 a)-d). These high energy pressure event distributions are for observation posts 1, 6, 4 and 5 respectively. The distributions cannot be analyzed rigorously based on shape since the curves are very noisy but noticeable peaks are visible. The extreme pressure distribution at mooring nodes 1 and 3, shown in Figures 5 a)-b), display strong peak values at the low time periods of 1.5-3 days. These are extreme wave fluctuations directly due to the hurricanes. Observation posts 4 and 5 displayed in Figures 5 a) and d), which are from mooring nodes 1 and 2, both show strong peaks at the period of 15 days. These high energy pressure events are most likely swell events propagating into the region over a two-week time scale after the hurricanes have officially dissipated.

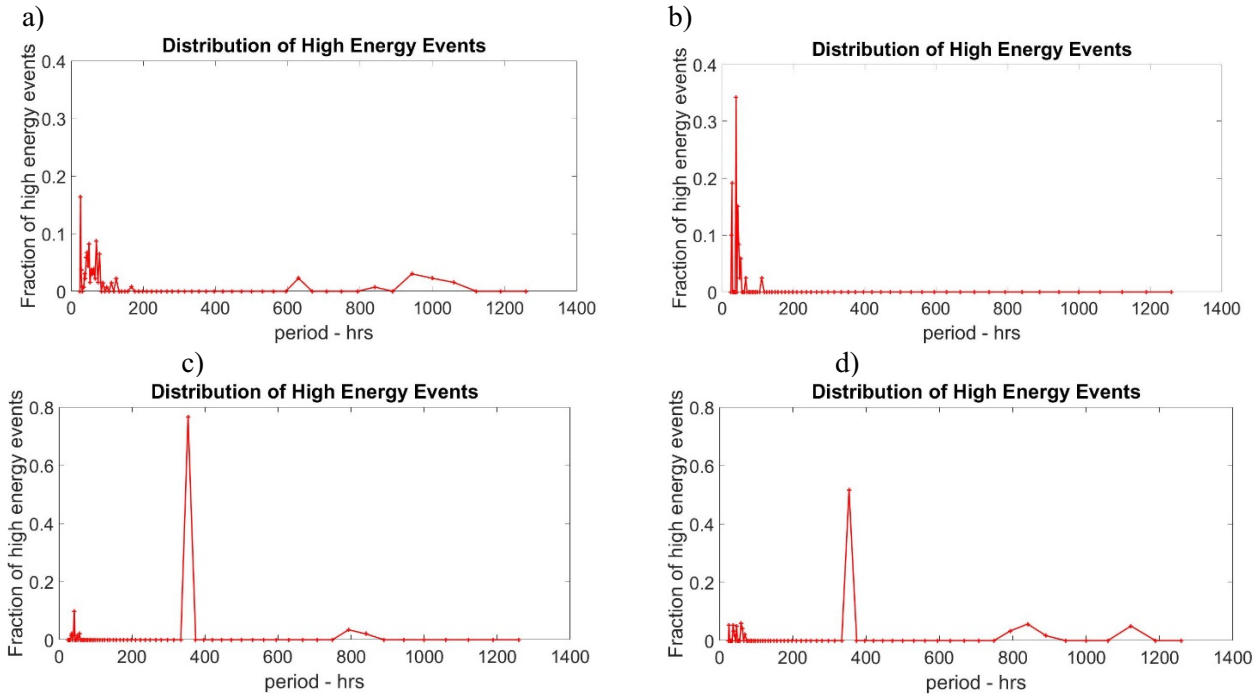

Figure 5: Extreme (maximum) value high energy pressure event statistics P_H captured at a) observation post 1, b) observation post 6, c) observation post 4, and d) observation post 5. Vertical axis is the average fraction of high energy pressure events. Horizontal axis is the time period scale in hours for the localized fluctuation associated with the Morlet wavelet. Distributions are scaled to sum to 1.

A BBN-based on the Chow-Liu algorithm can also be calculated using the maximum value pressure data matrices for the observation posts. Figure 6 displays the nodal-edge BBN map for these maximum pressure values. The histograms within the BBN nodes seem to have a Poisson shape which is consistent with an extreme nonlinear wave process quantified by the expected number of high-pressure events occurring within a fixed time interval at a constant mean rate. What is immediately noteworthy in the BBN is that not all the arrows emanating from the nodes point in the direction of the M2 or semidiurnal barotropic energy flux of west-to-east. Instead, two arrows, one emanating from observation post 5 and the other emanating from observation post 3, point from east-to-west. Because the hurricanes cause very confused seas, it is perfectly reasonable to observe significant wave signal information moving counter to the M2 barotropic energy flux. The mutual information value between observation posts 5 and 4 is 0.08 and the mutual information value between observation posts 3 and 2 is 0.05. This suggests that the wave signal information movement counter to the M2 barotropic energy flux is present but very weak. Most connections in the BBN are between adjacent mooring nodes of 1 and 2 and mooring nodes 2 and 3, but a connection between mooring nodes 1 and 3 does exist which is distant from one another at a scale of 83 km. This connection has a mutual information value of 0.06 which is also low suggesting that wave signal information movement in the original M2 tidal barotropic direction is also weak. Finally, mooring nodes 2 and 3 display downward propagation of energy with mutual information values of 0.06 and 0.07 respectively. This is consistent with the generation of waves at the ocean surface by hurricanes and the subsequent propagation of signal energy vertically into the water column. Overall, the structure of the BBN shows second order weak energy or information fluxes caused by extreme waves. The accrual of more data each year during the same season could provide mean spatial joint probabilistic distribution patterns allowing for the assessment of state change in a nodal area based on evidence provided at another.

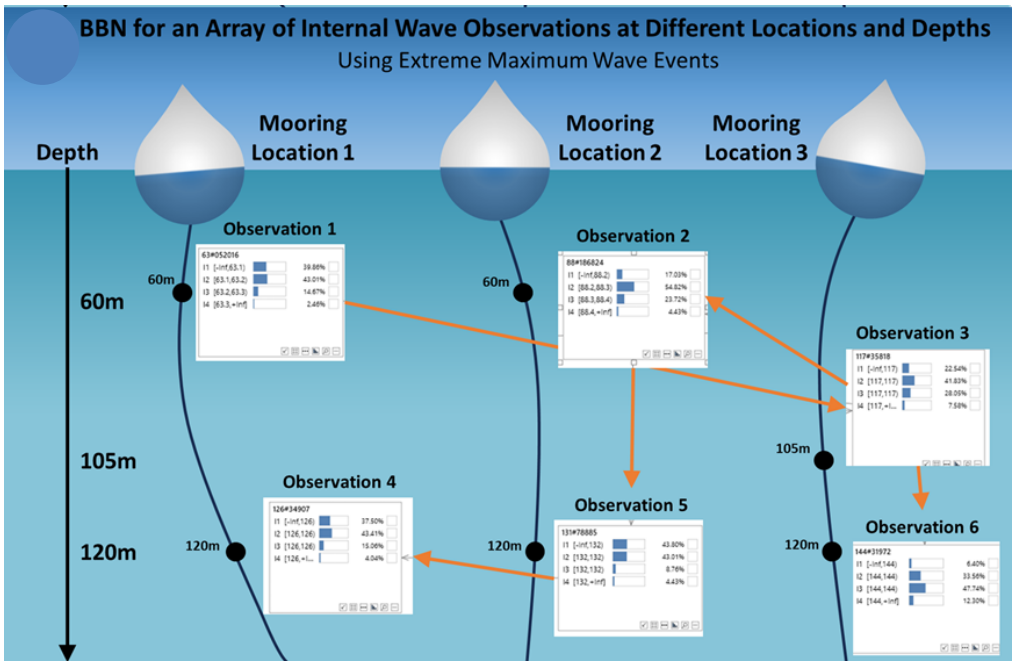

Figure 6: BBN for extreme maximum pressure value measurements captured by a mooring array situated off the northwest coast of Australia. Mooring nodes 1, 2, and 3 designated by vertical mooring columns of rectangular observations posts delineated by the rectangles. Pressure levels in arbitrary units are shown inside the rectangles. West and east are on left and right sides respectively. Depth labels for each observation post appear next to each rectangle. Edge connections displayed as arrows. No BBN evidential instantiations have been applied.

4. Conclusion

BBNs provide a practical means for the assessment of spatial interrelationships of sampling points embedded in complex internal wave fields. Structural learning via BBN analysis is a valuable way for characterizing ocean internal wave dynamical structure by displaying observation post covariance and the directions of information flow. The combination of low- and high-pressure internal wavefield components is spatially consistent with the anisotropic M2 barotropic energy flux direction where information moves from west-to-east over the continental shelf. Classical signal system identification along with Markovian modeling confirms this dynamic where noise laden filter and emission matrix structural results providing evidence of information propagation having a preferred direction consistent with BBN analysis. High pressure event statistics show spatial variability where peaks delineate both short and long-time scales for high energy pressure events. Maximum pressure energy event distributions are consistent with the direct generation of extreme pressure internal waves over time scales of 1-3 days as well as residual pressure anomalies occurring over the much longer time scale of 15 days. These long-time scales are evidence of sea level fluctuations associated with the dissipation of hurricanes in the area. BBN analysis of the extreme internal wave pressure field reveals evidence of information flow in the opposite direction of the M2 barotropic energy flux as well as downward movement of energy illustrating the impact of hurricane dynamics. Longer term data acquisition combined with the application of BBN analysis could reveal information vital to making statistical inferences regarding wave dynamics as well as other processes.

References

[1] J. W. Book, N. L. Jones, R. J. Lowe, G. N. Ivey, C. R. Steinberg, R. M. Brinkman, A. E. Rice, C. E. Bluteau, S. R. Smith, T. A. Smith, and S. Matt, "Propagation of Internal Tides on the Northwest Australian Shelf Studied with Time-Augmented Empirical Orthogonal Functions," in *20th Australasian Fluid Mechanics Conference*, Perth, Australia, December 5-8, 2016.

[2] K. B. Korb and A. E. Nicholson, *Bayesian Artificial Intelligence*. Florida, USA: CRC Press, 2010.

[3] U. B. Kjaerulff and A. L. Madsen, *Bayesian Network and Influence Diagrams: A Guide to Construction and Analysis.* New York, NY: Springer, 2008.

[4] A. Darwiche, *Modeling and Reasoning with Bayesian Networks*. New York, NY: Cambridge University Press, 2009.

[6] W. L. Martinez, and A. R. Martinez, *Computational Statistics Handbook with MATLAB, Third Edition*. Boca Raton, FL: Chapman and Hall/CRC, 2015.

[7] O. C. Ibe, *Markov Processes for Stochastic Modeling*, Second Edition, New York: NY: Elsevier, 2013.

[8] G. Fink, *Markov Models for Pattern Recognition: From Theory to Applications*, New York, NY: Springer, 2014.

[9] P. S. Addison, *The Illustrated Wavelet Transform Handbook: Introductory Theory and Applications in Science, Engineering, Medicine and Finance*, New York: NY, Taylor and Francis Group, 2002.

[10] A. Grinsted, J. C. Moore, and S Jevrejeva, "Application of the Cross Wavelet Transform and Wavelet Coherence to Geophysical Time Series," *Nonlinear Processes in Geophysics*, Vol. 11, 564-566, 2004.

[11] N. Scott, "Estimating Steep Wave Statistics Using a Wave Gauge Array," *Applied Ocean Research*, New York: NY, Elsevier, Vol. 27, pp. 23-38, 2005.

[12] N. Scott, T. Hara, E. J. Walsh, and P. A. Hwang, "Observations of Steep Wave Statistics in Open Ocean Waters," *Journal of Atmospheric and Oceanic Technology*, Vol. 22, 3, pp. 258-271, 2005.

[13] N.V. Scott, and T Kulkulka, "Bayesian Belief Network Analysis of a Large Eddy Simulated Ocean Turbulence Field," in *Proceedings of the 9th International Conference on Fluid Flow, Heat, and Mass Transfer*, No. 175, doi:10.1159/ffhmt22.175.

[14] L. R. Vega, *A Rapid Introduction to Adaptive Filtering*. New York, NY: Springer, 2013.

[15] S. Coles, *An Introduction to Statistical Modeling of Extreme Values.* New York, NY: Springer, 2001.